JBR–BTR, 2011, 94: 319-329.

NON-INVASIVE GRADING OF ASTROCYTIC TUMOURS FROM THE RELATIVE CONTENTS OF MYO-INOSITOL AND GLYCINE MEASURED BY IN VIVO MRS

A.P. Candiota[1,2], C. Majós[3,1], M. Julià-Sapé[1,2,4], M. Cabañas[5,1], J.J. Acebes[6,1], A. Moreno-Torres[7,1], J.R. Griffiths[8], C. Arús[2,1,4]

MRI and MRS are established methodologies for evaluating intracranial lesions. One MR spectral feature suggested for in vivo grading of astrocytic tumours is the apparent myo-Inositol (ml) intensity (ca 3.55ppm) at short echo times, although glycine (gly) may also contribute in vivo to this resonance. The purpose of this study was to quantitatively evaluate the ml + gly contribution to the recorded spectral pattern in vivo and correlate it with in vitro data obtained from perchloric acid extraction of tumour biopsies.

Patient spectra (n = 95) at 1.5T at short (20-31 ms) and long (135-136 ms) echo times were obtained from the INTERPRET MRS database (http://gabrmn.uab.es/interpretvalidateddb/). Phantom spectra were acquired with a comparable protocol. Spectra were automatically processed and the ratios of the (ml + gly) to Cr peak heights ((ml + gly)/Cr) calculated. Perchloric acid extracts of brain tumour biopsies were analysed by high-resolution NMR at 9.4T. The ratio (ml + gly)/Cr decreased significantly with astrocytic grade in vivo between low-grade astrocytoma (A2) and glioblastoma multiforme (GBM). In vitro results displayed a somewhat different tendency, with anaplastic astrocytomas having significantly higher (ml + gly)/Cr than A2 and GBM.

The discrepancy between in vivo and in vitro data suggests that the NMR visibility of glycine in glial brain tumours is restricted in vivo.

Key-words: Astrocytoma - Magnetic resonance (MR), spectroscopy.

Abbreviation List

A2	Low-grade astrocytoma
A3	Anaplastic astrocytoma
GBM	Glioblastoma Multiforme
ml	Myo-inositol
Gly	Glycine
Cr	Creatine
NAA	N-acetyl aspartate
Cho	Choline
SW	Sweep width
TR	Recycling time
TE	Echo time
STE	Short time of echo
LTE	Long time of echo
PCA	Perchloric acid
HR-MAS	High resolution magic angle spinning
wtw	Wet tissue weight

MRI and MRS are well established methodologies for evaluating intracranial lesions (1,2). MRS is nowadays receiving increasing attention from radiologists and neurologists, and its use to help MRI in the clinical decision making process is increasing. MRS of brain tumours is currently used for diagnosis, grading, assessing therapeutic response and providing prognostic information on survival (3-4).

According to Stewart et al (5), approximately 60% of all intracranial tumours are of neuroepithelial origin (gliomas). Among the glioma subtypes, Chamberlain and Kormanik (6) have reported percentages of 40-50% for glioblastomas (GBM), 30-35% for anaplastic astrocytomas (A3), and 15-20% for low grade astrocytoma (A2). Proper grading of astrocytic tumours is important for the clinician to decide upon treatment and patient care (4, 6).

Current radiological methods do not distinguish adequately between the large number of recognised types of brain tumours, and histopathological diagnosis from a biopsy remains the gold standard for diagnosis and grading, although even here accuracy is not perfect (7). Neuroimaging-based classification (defined as the assignment of type and grade) is frequently reported to be unreliable, especially for certain lesions such as gliomas (8, 9). An additional non-invasive method for accurately diagnosing and grading brain tumours would be a major advance, particularly in those cases. As MRS spectra of brain tumours and other focal lesions are often quite distinctive, ^{1}H-MRS is a very promising non-invasive method for brain tumour diagnosis, and it is becoming widely acknowledged as a useful complement to MRI. Several *in vivo* diagnostic approaches for MRS have been tested, such as spectroscopic imaging (10) or single voxel MRS (11, 12). Previous studies with MRS have suggested correlations between metabolic features *in vivo* and the histopathological grade of astrocytic tumours (4, 13, 14), but they were generally concerned with the NAA, Cr and Cho resonances. In addition to those resonances, MRS produces much more information of potential interest for astrocytic tumour grading, e.g. the myo-inositol resonance (ca 3.55 ppm) which can be measured at short echo times (15-18).

It had earlier been realized that the J-modulation dependent effect on ml resonances would strongly decrease the apparent ml peak intensity at ca. 3.55 ppm (19). In contrast, since the gly resonance is a singlet and shows no J-dependent modulation, the ca. 3.55 ppm peak intensity will not be affected by echo time

From: 1.Centro de Investigación Biomédica en Red en Bioingeniería, Biomateriales y Nanomedicina (CIBER-BBN), Cerdanyola del Vallès, Spain, 2. Departament de Bioquímica i Biologia Molecular, Unitat de Bioquímica de Biociències, Edifici Cs, Universitat Autònoma de Barcelona, 08193, Cerdanyola del Vallès, Spain, 3. Institut de Diagnòstic per la Imatge (IDI), CSU de Bellvitge, Autovia de Castelldefels km 2.7, 08907, L'Hospitalet de Llobregat, Barcelona, Spain, 4. Institut de Biotecnologia i de Biomedicina (IBB). Universitat Autònoma de Barcelona, 08193, Cerdanyola del Vallès, Spain, 5. SeRMN, Edifici Cs, Universitat Autònoma de Barcelona, 08193, Spain, 6. Department of Neurosurgery, Hospital Prínceps d'Espanya, CSU de Bellvitge, Feixa Llarga s/n, 08907, L'Hospitalet de Llobregat, Barcelona, Spain, 7. Research Department, Cetir Centre Mèdic SL-Unitat Esplugues, C/ Josep Anselm Clavé 100, 08950 Esplugues de Llobregat, Spain, 8.Cancer Research UK, Cambridge Research Institute, Robinson Way, Cambridge CB2 ORE, UK.

Address for correspondence: Dr C. Arús, Departament de Bioquímica i Biologia Molecular, Unitat de Bioquímica de Biosciènces, Edifici Cs, Universitat Autonoma de Barcelona, 08193, Cerdanyola del Vallès, Spain. E-mail: carles.arus@uab.es

when gly is its major contributor. Barba et al (20) utilised this echo time J-coupling modulation-dependent effect to estimate the relative ml and Gly content in human brain tumours *in vivo*. This approach was extended using a two-phantom protocol to produce an expression that should allow estimation of the MRS visible ml/gly content ratio (21).

We now report the use of a simple expression for ml + gly content relative to creatine content for astrocytic tumour grading from in vivo MRS data, and an investigation of a biochemical rationale for this method, based on the analysis of biopsy metabolite extracts by high field NMR spectroscopy.

Methods

Patients

The *in vivo* MRS data from patients involved in this study were acquired by the INTERPRET project (http://azizu.uab.es/INTERPRET) at the following centres: St George's Hospital Medical School (SGUL), Institut de Diagnòstic per la Imatge CSU Bellvitge (IDI), Centre Diagnòstic Pedralbes (CDP), Fundación para la Lucha contra las Enfermedades Neurológicas de la Infancia (FLENI), Medical University of Lodz (MUL). The Institutional Review Board of each institution approved the study and patients gave signed informed consent prior to the MRS exploration.

Biopsy samples (n = 74; A2 n = 7, A3 n = 8, GBM n = 59) were collected after surgical resection of tumours at Hospital Universitari de Bellvitge. The Institutional Review Board approved the study and patients gave signed informed consent prior to surgery. Samples were frozen in liquid nitrogen within 5 minutes of collection and maintained in those conditions until processing at the Universitat Autònoma de Barcelona (UAB). The Anatomical Pathology department of the hospital provided the diagnosis of the patient.

For the *in vivo* MRS cases, the histopathological diagnosis was achieved by examination of a biopsy sample from the tissue excised at operation. Diagnostic agreement was required between a minimum of two of the consultant neuropathologists involved in the INTERPRET project (see (11) for further details). For the unpaired cases (no MRS, but biopsy collected), the local pathologist's diagnosis was used.

Perchloric acid extraction of biopsies

Perchloric acid (PCA) extracts were carried out essentially as in (22). Frozen samples were pulverized with a pre-cooled mortar and pestle. The fine powder obtained was transferred into a tube containing 0.5 M PCA (6 ml/g wet weight) and homogenized. External fumarate (ca. 5 µmol/g wet weight) was added as an internal standard to account for extraction process losses (23). Samples were centrifuged to eliminate precipitated potassium perchlorate (40,000 x g for 15 min), re-extracted once and supernatants combined and freeze-dried. All operations were performed at 4°C. The PCA-insoluble pellet was kept for further protein analysis. Prior to NMR acquisition, samples were resuspended in 400 ml of D_2O. The pH* (pH meter reading uncorrected for the deuterium isotope effect) was adjusted to 7.06 ± 0.22 and TSP (3-trimethylsilyl- 2,2,3,3- sodium tetradeuteropropionate) was added as chemical shift and concentration standard (final concentration of TSP proportional to the initial frozen sample weight). Some samples had been analysed by the group previous to the introduction of the internal standard into the extraction protocol; they were corrected for the mean losses (25%) observed in our present PCA protocol which includes an internal standard (24).

In vivo MRS spectra

Patient spectra (n = 95; A2 n = 18, A3 n = 7, GBM n = 70) were obtained from the INTERPRET validated database (http://gabrmn.uab.es/interpret-validateddb <accessed on 2011-01-21>). The consensus protocols developed by the INTERPRET project for acquisition of MRI and MRS data (25) are shown in Table I. Gadolinium contrast agents, when used, were given prior to MRS measurements. The MRS voxel was

Table I. — Consensus acquisition protocols for new data and also ranges (in italics) used for retrospective data accepted into the INTERPRET database. Mixing time in STEAM sequences (short echo time) varied and was the standard for the different systems used.

PARAMETER	STEAM (SHORT TE)	PRESS (SHORT TE)	PRESS (LONG TE)
TE	20 ms (*20-32 ms*)	30 -32 ms (*30-32 ms*)	136 ms (*135-144 ms*)
TR	2000 ms (*1600-2000 ms*)	2000 ms (*1600-2000 ms*)	2000 ms (*1600-2000 ms*)
Volume	4-8 cm^3	4-8 cm^3	4-8 cm^3
N. averages metabolites	256	192-128	192-128
N. averages water	8 to 32	8 to 16	8 to 16
N. points	512 [Philips] 1024 [Siemens] 2048 [GE]	512 [Philips] 1024 [Siemens] 2048 [GE]	512 [Philips] 1024 [Siemens] 2048 [GE]
Bandwidth	1000 Hz [Philips] 1000 Hz [Siemens] 2500 Hz [GE]	1000 Hz [Philips] 1000 Hz [Siemens] 2500 Hz [GE]	1000 Hz [Philips] 1000 Hz [Siemens] 2500 Hz [GE]
Dummy scans	4	4	4

Table II. — Glycine, myo-Inositol and creatine concentrations in the phantom used for the calibration curve.

Phantom number	[mI] (mM)	[Gly] (mM)	Ratio [mI/Gly]	[Cr] (mM)
1	0	80	0	10
2	12	78	0.15	10
3	16	64	0.25	10
4	27	54	0.5	10
5	40	40	1	10
6	54	27	2	10
7	60	12	5	10
8	70	7	10	10
9	80	5	16	10
10	80	0	∞	10

placed on the cellular part of the tumour, according to the previous MRI exploration.

Phantom studies at clinical field

Phantom studies were planned from calculations based on the concentration ranges and T_2 of brain metabolites (mI, gly, Cr) reported by others (26-28), as well as previous experimental data from our group (20), and were devised in order to estimate by previous external calibration the mI/gly ratio *in vivo*. The calibration curve solution had a constant creatine concentration (10 mM) and variable mI and gly concentrations (Table II). The phantom used in these acquisitions was based on the EUROSPIN phantom, and is described in more detail in (29).

Acquisition of phantom spectra (inner phantom cube containing the model solutions described in Table II) was carried out in a Philips scanner (ACS NT) operating at 1.5 T. MRS; acquisition parameters were: PRESS sequence, 512 data points, SW 1000 Hz, TR 2 s, TE 30 and 136 ms. The number of acquisitions was 96 for short TE (STE) and 128 for long TE (LTE), except in the case of the phantom with a lower concentration of mI (12 mM) in which the number of acquisitions was increased to 768. The single voxel (SV) volume was placed inside the inner cube of the phantom and the voxel size was fixed to 1.5 cm^3. Unsuppressed water reference spectra were also acquired with the same parameters except that the number of acquisitions was 16.

In vitro high resolution NMR spectroscopy

Pulse-and-acquire spectra were acquired in an ARX - 400 spectrometer operating at 9.4 T (Bruker SADIS, Wissembourg, France) at the UAB facility 'Servei de Ressonància Magnètica Nuclear' (SeRMN) at 298 K. Acquisition parameters were: time domain 16 k (8 k complex points), sweep width 4854 Hz, recycling time 10 s, and water presaturation with 0.05 mW power for 1 second. Initially, a short spectrum (16 scans) with 30s of recycling time was acquired to allow for fumarate quantification and loss-related corrections. The number of acquisitions was between 64 and 4096 scans, depending on the initial biopsy sample weight. Spectra were processed with DC correction, zero filling to 16 K and 0.3 Hz line broadening before Fourier transformation with WINNMR version 6.1.0.0 (Bruker Daltonik, GmbH) in a PC. Peaks of interest were fitted to Lorentzian-shaped curves, quantified with respect to the TSP reference with WINNMR, and finally corrected for the percent losses measured or estimated from fumarate content in the final extract sample.

Processing of in vivo MR spectra

In vivo and phantom spectra were automatically processed with a software module derived from the INTERPRET data manipulation software (11, 12). This module carried out the required functions such as Fourier transform, residual water filtering by HLSVD between 4.3 and 5.1 ppm, offset correction, zero order (Klose algorithm) phase correction, setting the 4.2 to 5.0 ppm range to zero, exponential apodisation resulting in a line broadening of 1Hz and normalization of the spectra to Euclidean unit length (eq.1), with X being the height of any point in the spectral vector. Next, the signal-to-noise ratio (SNR) for the tallest peak in the 0-3.4 ppm range was also calculated (see (11) and (12) for further details). The noise level was defined as the average standard deviation of noise between 9 to 11 ppm. The resulting processed file had 512 points and ranged from -2.7 to 7.1 ppm. Astrocytoma cases in the database were only used if they had available both one short echo and one long echo time spectrum, which had both passed spectroscopic quality control criteria (water linewidth at half height < 8 Hz and SNR > 10, and lack of visible spectral artifacts (11)).

$$\frac{X^2}{\sqrt{\sum_{i=1}^{i=n} X^2}} \qquad [1]$$

An additional inclusion criterion for this work (but see also (29)) was that only spectra with SNR higher than 5 for the 3.55 ppm (mI + gly) and 3.03 ppm (creatine) signals at short echo time (STE) spectra were used. Following these restrictions, 9 spectra (1 A2 and 8 GBM) were discarded.

In order to make the (mI + gly)/Cr function simple to measure, we used peak heights rather than peak areas. In principle a non-specialist user of the method could measure them with a pencil and ruler. In the present study, a modified processing module was developed to calculate SNR and peak heights for *in vivo* and phantom spectra. The 3.03 and 3.55 peak heights and their SNR (range -2 to -1 ppm as basis) were automatically calculated for STE and long echo time (LTE) for the resulting processed file derived from the INTERPRET data manipulation software (DMS).

Before peak height measurement in phantom spectra, a 4 Hz line broadening was applied to mimic the linewidth effects in *in vivo* brain tumour spectra. After that, the (mI + gly)/Cr ratio (eq.2) was calculated.

$$\frac{\left[\frac{(3.55\ \text{ppm}\ \textit{height STE})}{(3.03\ \text{ppm}\ \textit{height STE})}\right]}{\left[\frac{(3.55\ \text{ppm}\ \textit{height LTE})}{(3.03\ \text{ppm}\ \textit{height LTE})}\right]} = (\text{mI} + \text{gly})/\text{Cr} \qquad [2]$$

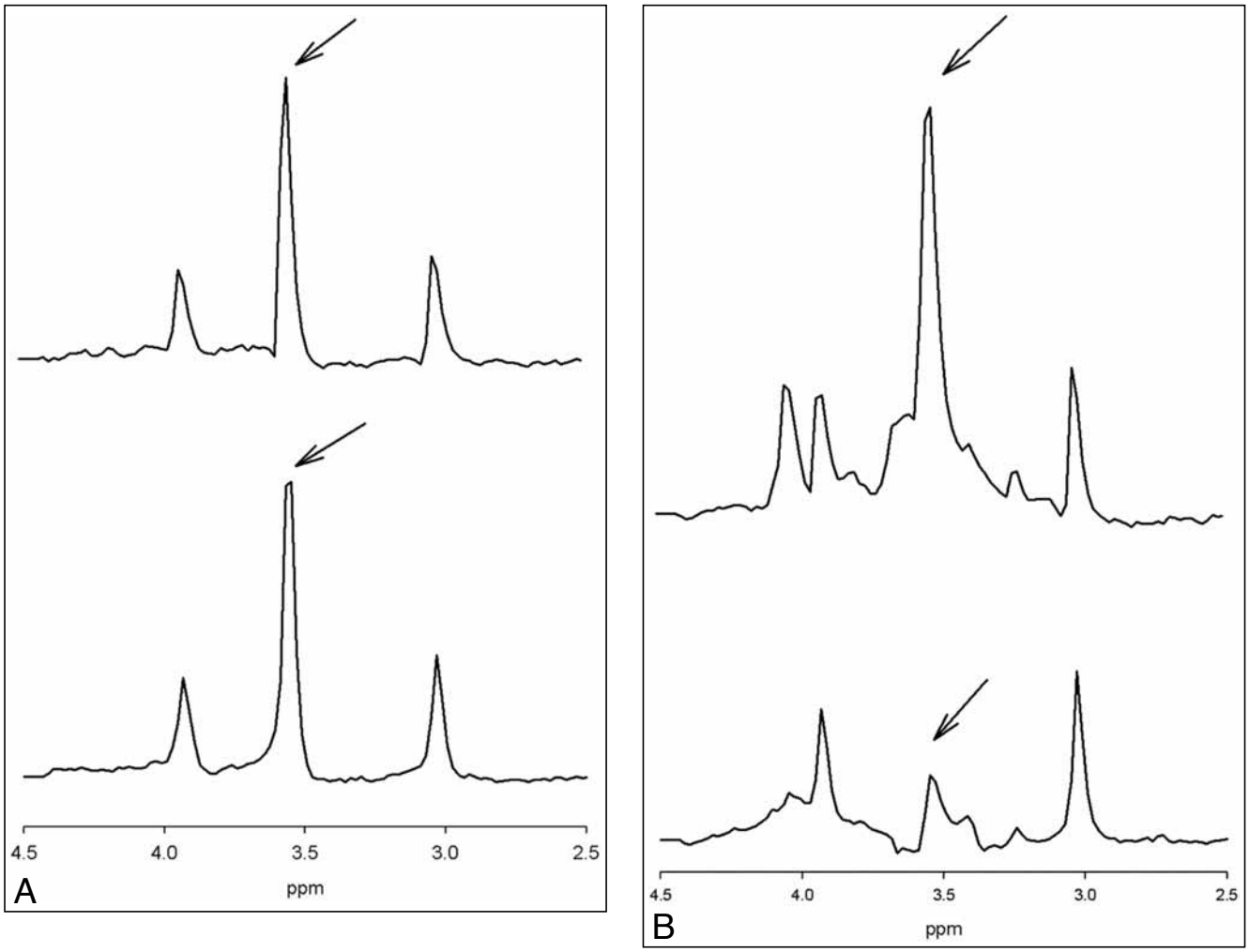

Fig. 1. — Spectra at STE (top) and LTE (bottom) at 1.5 T of phantom solutions of two calibration curve points. A) phantom #1: creatine 10 mM, gly 80 mM and B) phantom #2: creatine 10 mM, ml 12 mM. The ml/gly peak at ca 3.55 ppm is labelled with an arrow. Phantom spectra were scaled to approximately constant creatine peak height for each pair of STE/LTE spectra.

Simulation of expected (ml + gly)/Cr from in vitro PCA extract calculated values

The (ml + gly)/Cr that would be expected *in vivo* was simulated from *in vitro* PCA extract sample data. This simulation was based in data obtained with the phantom calibration curve and an equation (equation 3, see results) was adjusted to give curve points that correlate the (ml + gly)/Cr *in vivo* to ml and gly concentrations measured *in vitro*.

Statistical analysis

Statistically significant differences were evaluated as follows: the normal distribution of values was assessed with the Kolmogorov-Smirnov test and the variance homogeneity with the Levene's test. Values with a normal distribution and homogeneous variance were compared with Student's t test or (if more than two comparisons were carried out) the ANOVA test. For values with normal distribution but inhomogeneous variance, Student's t-test was carried out.

Values with non-normal distribution were evaluated with the non-parametric Mann-Whitney's U test. Significance level was set to 0.05, and all analyses were carried out with SPSS version 11.5.1 and 14.0 (SPSS Inc, Chicago, IL).

Results

Phantom studies and calculation of (ml + gly)/Cr

Phantom spectra were acquired under conditions of good SNR, which allowed clear identification of peaks of interest (see figure 1). The SNR range obtained for the signals of interest was 30-122 (STE) and 51-78 (LTE).

The ml signal at LTE was attenuated when compared to the creatine signal, due to ml J-coupling induced phase modulation, whereas glycine remained practically isointense with respect to creatine at 3.03 ppm (Fig. 1). Values of calculated ml and gly concentrations used in the phantom and the resulting (ml + gly)/Cr ratio were used to devise the calibration curve shown in figure 2. From these values, an asymptotic equation was obtained from fitting the calculated (ml + gly)/Cr for each (ml)/[gly] ratio (eq. 3), with the SIGMAPLOT (Systat Software) program.

$$y = \frac{5.02}{1 + \exp\left(\frac{-(x - 2.77)}{3.11}\right)} \quad [3]$$

From equation [3], (ml + gly)/Cr (y) values *in vivo* can be predicted

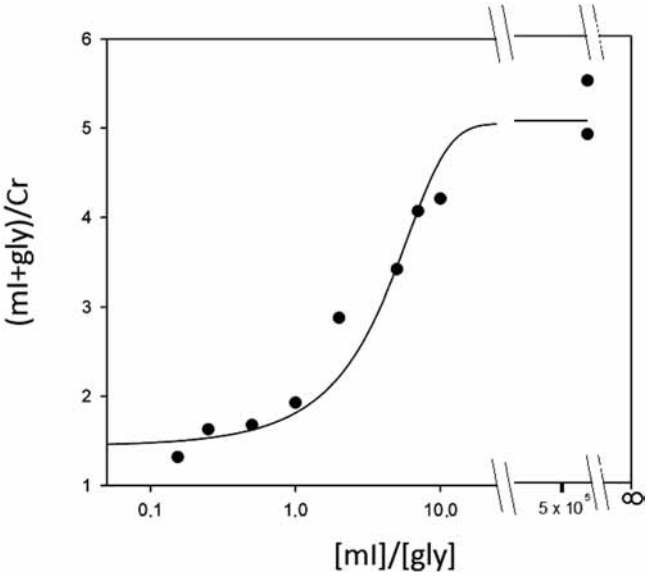

Fig. 2. — Calibration curve (semilogaritmic plot) obtained with phantom measurements. For proper fitting, an arbitrary value of 500,000 was used in place of "∞" for (mI)/[gly] in phantom solution #10, for which two different acquisitions were performed. The value for phantom #1 is not shown in the plot.

from assumed mI and gly content ratios (x), and vice versa mI/gly ratios calculated from *in vivo* measured (mI + gly)/Cr.

In vivo measurement of (mI + gly)/Cr for calculation of (mI)/[gly)

The initial set of *in vivo* spectra (n = 95) available in the database was reduced to n = 86 by application of the criteria mentioned previously: unsuppressed water linewidth and SNR for the whole spectral pattern, and for the individual 3.55 and 3.03 peaks. Variations due to short echo time STEAM or PRESS sequences (STE) were assessed by separating cases according to acquisition conditions and testing (t-test) for differences between groups (data not shown), and no significant differences were found. This observation agrees with that of Ernst and Hennig (19), who reported differences in modulations between metabolites measured with STEAM and PRESS sequences, but only at higher echo times (> 50 ms). Slight differences in echo time (20-35ms for STE or 135-136 ms for LTE) were assumed to be negligible for the purposes of this work with respect to MRS pattern effects in the mI/gly or Cr regions. Table III summarizes (mI + gly)/Cr and (mI)/[gly) calculation from equation 3 for the studied groups (A2, A3 and GBM).

The distribution of glial cases in the validated INTERPRET database that fulfilled the inclusion criteria for this analysis partially agrees with the distribution reported in (6), in which of 86 astrocytoma cases, 72.1% were glioblastomas, 8.1% were anaplastic astrocytomas and 19.8% were diffuse astrocytomas. The agreement is even more complete if high grade (GBM + A3) tumours are compared with low grade (A2) tumours; the numbers are then 80.2% vs. 19.8% in the INTERPRET data and 70-85% vs. 15-20% in (6). In typical *in vivo* spectra (Fig. 3A and 3B, mean spectra), the attenuation of the 3.55 ppm signal at LTE is higher in low-grade tumours, whereas in glioblastomas, there is usually little attenuation. Furthermore, the boxplot in figure 4A shows that (mI + gly)/Cr tends to be inversely correlated with grade, achieving statistically significant differences between A2 and GBM.

The (mI + gly)/Cr values obtained for paired *in vivo/in vitro* cases (most of which, 15/16, were GBMs, Table IV) were variable; some cases presented similar values and some cases did not. These values were statistically compared with Student's "t" test and significant differences ($p = 0.02$) were found. The (mI + gly)/Cr value tended to be higher *in vivo*, suggesting a lower apparent glycine content *in vivo*.

Gly and mI content in biopsies from in vitro measurements of PCA extracts and calculation of the predicted (mI + gly)/Cr in vivo

Typical PCA extract spectra from biopsies can be seen in figure 5, with examples of spectra from A2 and GBM. Values for (mI)/[gly) were calculated for each *in vitro* spectrum, and equation 3 was used for predicting the expected (mI + gly)/Cr value *in vivo*. Average values for gly and mI concentration ratios obtained from biopsies are summarized in Table V. The total number of paired cases (MRS and biopsy extraction) is summarized in Table IV.

The boxplot for the calculated (mI + gly)/Cr is shown in figure 4B and in Table III a statistically significant decrease in (mI + gly)/Cr between A3 and GBM can be seen, while the reverse tendency is observed between A2 and A3, the former presenting lower values.

While the (mI + gly)/Cr values for GBM and A3 are not significantly different when comparing values measured *in vivo* with values calculated from extract data, (mI + gly)/Cr values for A2 are significantly different, being 3-fold lower for *in vivo* data with respect to ratios calculated from *in vitro* data (Table III).

Discussion

Quantification of the mI/gly ratio in vivo by combining data acquisition at two echo times

Several approaches have been used to evaluate the mI and/or gly content of the human brain and of human brain tumours using data obtained *in vivo* in clinical scanners (1.5-7T) (20, 30-35). This measurement is difficult, especially at low field, because of the co-resonance at ca. 3.55 ppm of the singlet resonance of glycine with the J-coupled resonances from the protons of myo-inositol (protons 1, 3, 4 and 6). Most authors have usually resorted to independent gly and mI quantification at a single echo time (between 30 and 144 ms (31, 33, 34)) or have used a method based on averaging echo time results in the 30-284 ms range (31, 36), and using frequency domain fitting and quantification with LCModel. The method described in (31, 36) was also based on the well known fact that the J-modulation dependent effect on mI resonances would strongly decrease the apparent mI peak intensity at ca. 3.55 ppm at short TE (15, 19, 20). Additionally, since the gly resonance

Table III. — Measured (ml + gly)/Cr (in vivo) or calculated from biopsy data (in vitro) and (ml)/[gly] calculated (in vivo) or measured from biopsies (in vitro). Values are mean ± SD.

	In vivo			*In vitro*		
	A2 n = 17	A3 n = 7	GBM n = 62	A2 n = 7	A3 n = 8	GBM n = 59
(ml + gly)/Cr [a,b,c]	6.08 ± 3.42	4.28 ± 2.30	2.91 ± 3.00	2.36± 0.62	3.53± 1.14	2.12 ± 0.60
[ml]/[gly] [d,e,f]	17.06 ± 9.49	10.10 ± 9.90	5.35 ± 8.67	2.39 ± 1.59	6.28 ± 3.90	1.89 ± 2.23

(a) $p < 0.05$ for in vivo/in vitro comparisons (A2 x A2 values)
(b) $p < 0.05$ for in vivo comparisons (A2 x GBM values)
(c) $p < 0.05$ for in vitro comparisons (A2 x A3 and A3 x GBM values)
(d) $p < 0.05$ for in vivo/in vitro comparisons (A2 x A2 values)
(e) $p < 0.05$ for in vivo comparisons (A2 x GBM values)
(f) $p < 0.05$ for in vitro comparisons (A2 x A3 and A3 x GBM values)

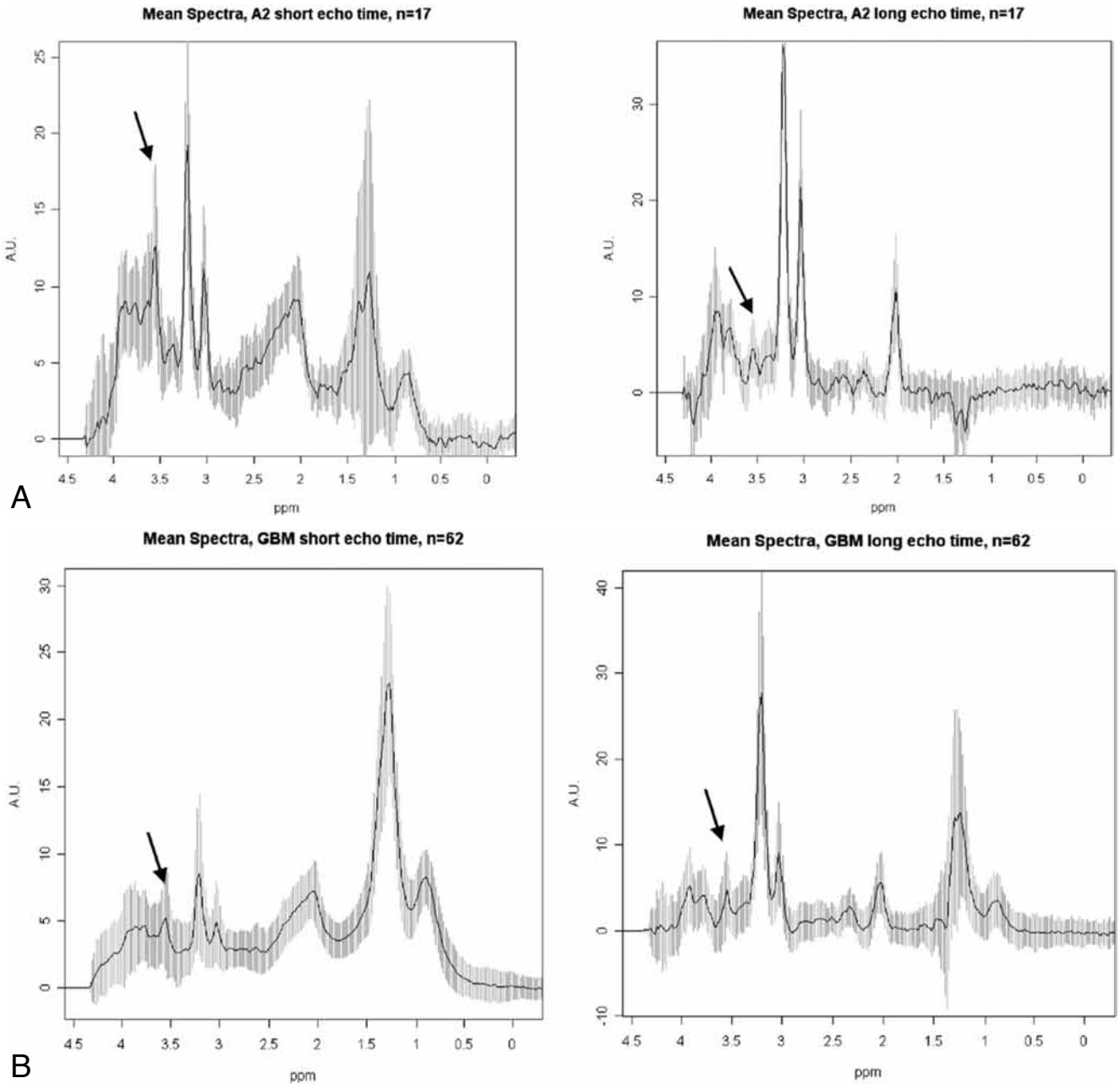

Fig. 3. — In vivo mean spectra + /- SD (shading) at STE (left) and LTE (right) for A) A2 cases (n = 17) and B) GBM cases (n = 62). Note that for the A2 cases, the 3.55 ppm signal (arrows) is high at STE and much lower at LTE, whereas for the GBM the relative signal height with respect to creatine at 3.03 ppm remains high. Spectral intensity was set to zero after 4.2 ppm to avoid contribution of artefactual signal due to suboptimal water suppression (11).

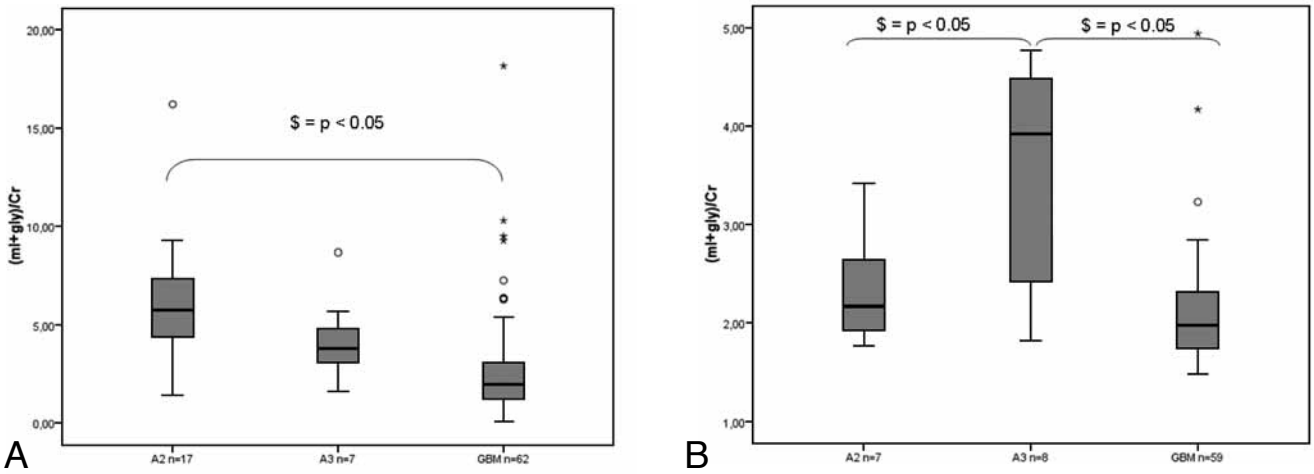

Fig. 4. — A) Boxplot for (ml + gly)/Cr automatically calculated from actual *in vivo* spectra ($) labels significant differences using an ANOVA test between the A2 and GBM groups. Number of cases for each group is given on the abscissa axis. B) Boxplot obtained for predicted (ml + gly)/Cr *in vivo*, calculated from values obtained from PCA extracts of biopsies. ($) labels significant differences between the A3 and the other two groups. In these boxplots, upper and lower box limits represent 3rd and 1st quartiles, respectively. The central thick line is the median. Whiskers label maximum values comprised between the quartile and the product Interquartile Range (IQR) x 1.5. Outliers are represented as circles when value is within the 1.5 and 3.0 x IQR. Extreme outliers (higher than 3.0 x IQR) are represented as *.

is a singlet and shows no J-dependent modulation, the ca. 3.55 ppm peak intensity is not affected by echo time when gly is its major contributor. This effect had already been noticed in studies of glial tumours *in vivo* (15, 20). Barba et al (20) used the echo time J-coupling modulation-dependent effect to estimate the relative ml and gly content of human brain tumours (hemangioperycitomas and meningiomas) *in vivo*. In that study, ml/gly content was estimated from a two phantom protocol. This approach has been extended in our present work (see also (21) for a preliminary description) to produce an expression (equation 3) that allows MRS-visible ml/gly content ratio estimation under our experimental conditions. No correction was applied in our work for possible differences in T1 or T2 values between the phantom solution and brain tumour tissue. Accordingly, the ml/gly ratio calculated for the tumour tissue should be considered an approximation to the real tissue ml/gly. If T1 or T2 values differentially change for ml and gly, this could produce an apparent ml/gly ratio derived from the measured ratio, weighted by the relative NMR visibility of the two compounds, and compared with the height of a singlet resonance which is not affected by the echo time modulation (creatine). A similar approach to the present one was described by Hattingen et al. (35) for MRSI dataset grids. They also used the change in pattern produced by recording spectra from human brain tumours at two echo times (30 and 144 ms), time domain data fitting using AMARES and QUEST, and phantom spectra, to calculate ml/gly ratios for low grade astrocytomas (A2), high grade astrocytomas (A3 + GBM) and control subjects (35). Their results, which would be qualitatively equivalent to 1/(ml + gly)/Cr using the terminology in our study, also showed a trend to increasing apparent gly content in high grade tumours, although a full quantitative comparison between both studies is made difficult by the different phantom approach used and their combination of A3 (n = 10) and GBM (n = 5) in a single high grade group. The approach described herein may have some advantages with respect to other previously developed approaches in its relative simplicity, which should allow its use with SV MRS data acquired at any clinical centre. Monitoring of the relative ml/gly content *in vivo* may also be of interest for other clinical conditions in which changes in the relative contents of ml or gly are expected (20, 34, 36).

Relevance of the apparent ml and gly content detected by MRS in vivo for non-invasive astrocytic tumour grading

The relative content of ml and gly in tumours was calculated ((ml + gly)/Cr) from the quantitative pattern change caused by the MRS visibility of ml varying at increasing echo times (19, 20). The apparent ml/gly ratio obtained *in vivo* (Fig. 4A) by substituting the experimental values into equation 3 has allowed us to demonstrate statistically significant differences in calculated ml/gly ratios between low grade astrocytic tumours (n = 17) and glioblastoma multiforme (n = 62) (Table III). This would agree with previous work (17) in which a tendency for a higher ml/Cr to be associated with lower grade had already been described at a single echo time (20 ms) in a smaller cohort of patients (n = 34), albeit without statistical analysis of the differences described. However, even though a trend towards a decrease in ml/gly ratio with grade exists (Fig. 4A) and statistically significance can be demonstrated for the difference between A2 and GBM, there is a great deal of overlap among grades. Therefore, if the (ml + gly)/Cr value is to be used for tumour grading, it should be combined with other relevant spectral features that have already been described (11, 37, 38). Indeed, the ml + gly peak height or peak area have already been used for classifier development at short (ca. 30 ms) or long (ca. 136 ms) echo times (11, 16, 37), and a joint classifier that uses information from the two echo times has recently been developed (39). We have already pointed out (37) that the manual combination of data obtained at short and long echo time significantly improves human brain tumour classification, and also the grading of astrocytic tumours. The (ml + gly)/Cr factor described here would

Table IV. — Number of paired cases (in vivo MRS + in vitro biopsy extract) in this study.

Pathology	Total number of cases	Number of paired cases (%)
A2	17	1 (5.8%)
A3	7	0 (0%)
GBM	62	15 (24%)

Table V. — In vitro (PCA extracts) values of glycine and myo-Inositol (mean ± standard error of the mean, µmol/gtw) calculated for biopsies.

	Glycine	myo-Inositol
A2 (n = 7)	1.98 ± 0.54	5.22 ±2.46
A3 (n = 8)	1.06 ± 0.29**	4.54 ± 0.75
GBM (n = 59)	3.28 ± 0.66	3.92 ± 0.55

**p < 0.05 for the comparison A3 vs GBM.

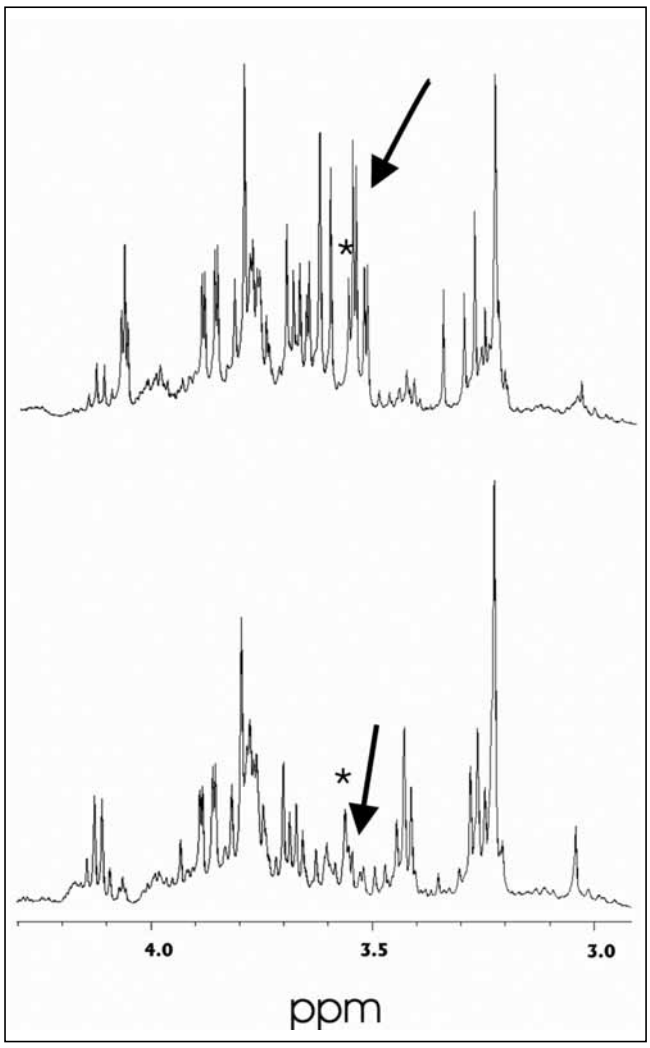

Fig. 5. — Typical biopsy extract spectra of a grade II astrocytoma (gly 1.34 µmol/gtw and ml 2.59 µmol/gtw) (top) and a glioblastoma multiforme (gly 2.18 µmol/gtw and ml 1.17 µmol/gtw) (bottom). Arrow points to part of the ml doublet of doublets (3.53/3.55 ppm) while star labels the gly singlet (3.56 ppm).

effectively combine the information contained in spectra obtained at the two echo times in the 3.55 ppm ml + gly region. Using a single echo time for astrocytic tumour grading may be misleading when using the 3.55 ppm region since, for instance, a signal that is high at short echo time would modulate and almost disappear at long echo time if it were due to ml, whereas it would be constant if it were due to gly. This confusion disappears if two echo times are used, as has previously been proposed (15, 20, 35). Noisy spectra can also cause overlap in calculated (ml + gly)/Cr -factor values , since the value of (ml + gly)/Cr will then approach one, independently of the grade investigated. In order to reduce the contribution of "bad quality" cases we therefore restricted our analysis to shortTE spectra with SNR values for the 3.55 and 3.03 ppm resonances that were larger than 5. A further reason for overlap in (ml + gly)/Cr data is that GBM is not a homogeneous tumour type: both tumour evolution and genetic data suggest that GBMs can be divided into primary and secondary groups (40), while transcriptomic studies have demonstrated three molecularly differentiated primary GBM subtypes (41). Although a detailed *in vivo* analysis of the MRS pattern of these GBM subtypes is still lacking, *ex vivo* data obtained by HR-MAS analyses of tumour biopsies suggest that secondary GBM could display a much higher ml content than primary ones (42). This would point to the possibility that the GBM outliers with a high (ml + gly)/Cr value in figure 4A could correspond to secondary GBMs. Further studies comprising survival data may be helpful in this respect.

Comparison of ml/gly calculated from in vivo data and ml/gly measured from biopsies in vitro

We were interested in validating the *in vivo* estimated ml/gly with *in vitro* data obtained from high resolution NMR spectra of PCA extracts from brain tumour biopsies. The glycine and ml contents in Table V show a similar trend compared to other reported studies (43-48): ml content decreased with astrocytic grade, albeit non-significantly, in agreement with (43-48). Furthermore, gly content increases with grade, in agreement with previous studies (43, 44, 46, 48) (gly was detected only in one out of five low grade astrocytoma cases analyzed

in (43)), and the same trend in gly increase with tumour grade was observed in (47 and 50) (HRMAS studies). In this respect, we are confident that our results from astrocytic tumour PCA extracts, obtained from the largest biopsy dataset yet described (n = 74), represent the expected metabolite pattern of the tumour grades investigated here. With respect to the discrepancy between (ml + gly)/Cr measured *in vivo* and calculated from *in vitro* data, there are several possible explanations. As biopsies and *in vivo* spectra were not matched (Table IV) it could be argued that sampling was somewhat biased. Furthermore, the biopsy sample may not necessarily represent the average spectral pattern sampled from a much larger voxel by the SV *in vivo* MRS approach. The rather large number of cases investigated (86 *in vivo* and 74 *in vitro*) makes this unlikely, as bias should not be coherent. Another possibility to take into account would be post-ischaemic changes in ml and or gly content between the *in vivo* tumour pattern and the pattern obtained from the PCA extract after open surgery resection of the biopsy. We are not aware that such changes have been described after the short ischaemia experienced by biopsies during the pre-freezing time (ca. 5 min) after surgical excision. One further possibility to take into account would be a reduced *in vivo* NMR visibility of gly in A2. If this were to be the case, the *in vivo* (ml + gly)/Cr value would be providing an apparent ml/gly ratio contributed only by the NMR-visible ml and Gly pools. One of the accepted causes of NMR invisibility of a small molecular weight metabolite is binding to macromolecular structures, with concomitant reduction of its T2 value (e.g. ADP bound to F-actin in muscle microfilaments). In this respect, binding of gly to multimeric channel proteins in the plasma membrane of PC-12 cells (50) or to a glycine-sensitive anion death channel in sinusoidal endothelial cells (51) have been proposed. Increased gly content protects various types of cells from necrotic or apoptotic death induced by ATP depletion (PC-12 cells, (51)), hypoxia (hepatic sinusoidal cells, (52)) or ischaemia-reperfusion derived reoxygenation injury (cardiomyocytes, (53)). As these are physiological situations usually encountered by tumours during progression, it would make sense if similar gly-derived effects were taking place. Then, since the gly pool in A2 tumours is smaller than in GBM, most gly would remain NMR invisible, bound to those plasma membrane proteins, perhaps due to a lower requirement for its protective effect. Once gly content increased above a certain threshold, or it was extracted by PCA, the NMR visibility would be recovered and the (ml + gly)/Cr would be correspondingly affected. In relation to this, it is worth mentioning here the recently described increase in apparent detection of Gly by HRMAS with increased recording time in GBM biopsies (48), which was also interpreted by the authors as suggesting higher gly visibility in GBM *ex vivo* with respect to the in the *in vivo* tumour MRS pattern. The concentration of gly that displays a protective effect in the various cell systems mentioned above is in the 3-5 mM range (51-53). This value is very close to the gly content found by us in GBM (3.28 μmol/gtw, Table V). Both explanations, the post-ischaemia changes and the reduced NMR visibility, could also account for some discrepancies observed between the expected (ml + gly)/Cr (deduced from *in vivo* data) and the calculated (ml + gly)/Cr (from *in vitro* data) for some of the paired cases in Table IV (results not shown).

It may be relevant to mention here that the ml/gly ratio has been analyzed in PCA extracts of rat glioma C6 cells (54) and has been found to be 3.2 times higher in post-confluent cells (ml/gly = 7.2, proliferation slowed down) than in log phase cells (ml/gly = 2.23, active proliferation). In this respect, actively proliferating C6 cells in culture would parallel the GBM behaviour, whereas proliferation-arrested C6 cells would partially mimic the situation in low grade astrocytic tumours. Therefore, changes in the ml/gly ratio in an astrocytic tumour *in vivo* with location (tumour heterogeneity) or progression towards malignancy could well be accessible non-invasively by monitoring changes in the (ml + gly)/Cr ratio.

Conclusions

An experimental protocol and an empirical formula have been developed to allow calculation of the (ml + gly)/Cr ratio from *in vivo* spectra of astrocytic human brain tumours. The *in vivo* (ml + gly)/Cr decreases with astrocytic tumour grade, and there is a statistically significant difference between the ratios in low grade astrocytoma and glioblastoma multiforme. The (ml + gly)/Cr ratio simulated from ml and gly concentration measured from PCA extracts of tumour biopsies suggest that part of the gly pool is not NMR visible *in vivo* in low grade astrocytomas. The (ml + gly)/Cr ratio may have application for astrocytic tumour grading and also for other cellular situations or pathologies in which the ml/gly ratio is expected to change.

Acknowledgements: We thank Lluís Martí and Guillem Mercadal for programming the SNR calculation automated module for *in vivo* spectra being analysed. We also thank Dr. Irene Martínez-Pérez and Dr. Ignasi Barba for the use of unpublished PCA extracts data. Work funded by MEDIVO (MCYT SAF 2002-00440), MEDIVO2 (MEC SAF2005-03650), PHENOIMA (MICINN SAF 2008-03323), Generalitat de Catalunya (2001 SGR-194, SGR2005 and XT2002-48) and INTERPRET (EU-IST-1999-10310). This work was also partially funded by the Centro de Investigación Biomédica en Red – Bioingeniería, Biomateriales y Nanomedicina, which is an initiative of the Instituto de Salud Carlos III (Spain) co-funded by EU FEDER funds. Data providers: Dr. C. Majós (IDI), Dr. A. Moreno-Torres (CDP), Dr. F.A. Howe and Prof. J. Griffiths (SGUL), Prof. A. Heerschap (RU), Prof. L Stefanczyk and Dr. J.Fortuniak (MUL), and Dr. J. Calvar (FLENI); data curators: Dr. A.P. Candiota, Dr. I. Olier, Ms. T. Delgado, Ms. J. Martín, M. Camisón and Mr. A. Pérez (all from GABRMN-UAB).

References

1. Danielsen E.R., Ross B.: Magnetic resonance spectroscopy diagnosis of neurological diseases. Marcel Dekker Inc, New York, 1999.
2. van der Graaf M.: In vivo magnetic resonance spectroscopy: basic methodology and clinical applications. *Eur Biophys J*, 2010, 39: 527-540.
3. Oh J., Henry RG., Pirzkall A., Lu Y., Li X., Catalaa I., Chang S., Dillon W.P., Nelson S.J.: Survival Analysis in Patients With Glioblastoma Multiforme: Predictive Value of Choline-to-NAcetylaspartate Index, Apparent Diffusion Coefficient, and Relative Cerebral Blood Volume *J Magn Reson Imaging*, 2004, 19: 546-554.
4. Fellows G.A., Wright A.J., Sibtain N.A., Rich P., Opstad K.S., McIntyre D.J., Bell B.A., Griffiths J.R., Howe F.A.: Combined use of neuroradiology and 1H-MR spectroscopy may provide an intervention limiting diagnosis of glioblastoma multiforme. *J Magn Reson Imaging*, 2010, 32: 1038-1044.
5. Stewart B.W., Kleihues P.: World Cancer Report. IARC Press, Lyon, 2003.
6. Chamberlain M.C., Kormanik P.A.: Practical guidelines for the treatment of malignant gliomas. *West J Med*, 1998, 168: 114-120

7. Coons S.W., Johnson P.C., Scheithauer B.W., Yates A.J., Pearl D.K.: Improving diagnostic accuracy and interobserver concordance in the classification and grading of primary gliomas. *Cancer*, 1997: 1381-1393.
8. Law M., Yang S., Wang H., Babb J.S., Johnson G., Cha S., Knopp E.A., Zagzag D.: Glioma grading: sensitivity, specificity, and predictive values of perfusion MR imaging and proton MR spectroscopic imaging compared with conventional MR imaging. *AJNR Am J Neuroradiol*, 2003, 24: 1989-1998.
9. Julià-Sapé M., Acosta D., Majós C., Moreno-Torres A., Wesseling P., Acebes J.J., Griffiths J.R., Arús C.: Comparison between neuroimaging classifications and histopathological diagnoses using an international multicenter brain tumor magnetic resonance imaging database. *J Neurosurg*, 2006. 105: 6-14.
10. De Edelenyi F.S., Rubin C., Estève F., Grand S., Décorps M., Lefournier V., Le Bas J.F., Rémy C.: A new approach for analyzing proton magnetic resonance spectroscopic images of brain tumors: nosologic images. *Nat Med*, 2000, 6: 1287-1289.
11. Tate A.R., Acosta D., Julià-Sapé M. et al : Development of a decision support system for diagnosis and grading of brain tumors using in vivo magnetic resonance single voxel spectra. *NMR Biomed*, 2006, 19: 411-434.
12. Pérez-Ruiz A., Julià-Sapé M., Mercadal G., Olier I., Majós C., Arús C.: The INTERPRET Decision-Support System version 3.0 for evaluation of Magnetic Resonance Spectroscopy data from human brain tumours and other abnormal brain masses. *BMC Bioinformatics*, 2010, 11: 581.
13. Kugel H., Heindel W., Ernestus R.I., Bunke J., du Mesnil R., Friedmann G.: Human brain tumors: spectral patterns detected with localized H-1 MR Spectroscopy. *Radiology*, 1992, 183: 701-709.
14. Ott D., Hennig J., Ernst T.: Human brain tumors: assessment with *in vivo* proton MR spectroscopy. *Radiology*, 1993, 186: 745-752.
15. Mader I., Roser W., Hagberg G.K., Schneider M., Sauter R., Seelig J., Radue E.W., Steinbrich W.: Proton chemical shift imaging, metabolic maps, and single voxel spectroscopy of glial brain tumors. *MAGMA*, 1996, 4: 139-150.
16. Majós C., Alonso J., Aguilera C., Serrallonga M., Pérez-Martín J., Acebes J.J., Arús C., Gili J.: Proton magnetic resonance spectroscopy (1H MRS) of human brain tumours: assessment of differences between tumour types and its applicability in brain tumour categorization. *Eur Radiol*, 2003, 13: 582-591.
17. Castillo M., Smith J.K., Kwock L.: Correlation of myo-inositol levels and grading of cerebral astrocytomas. *AJNR Am J Neuroradiol,*, 2000 21: 1645-1649.
18. Soares D.P., Law M.: Magnetic Resonance spectroscopy of the brain: review of metabolites and clinical applications. *Clin Radiol*, 2009 64: 12-21.
19. Ernst T.H., Hennig J.: Coupling effects in volume selective 1H spectroscopy of major brain metabolites. *Magn Reson Med*, 1991: 21: 82-96.
20 Barba I., Moreno A., Martínez-Pérez I., Tate A.R., Cabañas M.E., Baquero M., Capdevila A., Arús C.: Magnetic resonance spectroscopy of brain hemangiopericytomas: high myoinositol concentrations and discrimination from meningiomas. *J Neurosurg*, 2001, 94: 55-60.
21. Candiota A.P., Majós C., Julià-Sapé M., Cabañas M., Mercadal G., Acebes J.J., Moreno-Torres A., Griffiths J.R., Arús C.: M-Inositol and glycine content measurement for grading astrocytic tumours with *in vivo* MRS. In: Magnetic Resonance Materials in Physics, Biology and Medicine (MAGMA) 18 supplement 7 (Book of Abstracts ESMRMB, 2005 22nd Annual Scientific Meeting Basle/CH, Sept. 15-18, 2005): pp S 193, 2005. DOI: 10.1007/s10334-005-0002-2.
22. Rèmy C., Arús C., Ziegler A., Lai E.S., Moreno A., Le Fur Y., Decòrps M.: In vivo, ex vivo, and in vitro one- and two-dimensional nuclear magnetic resonance spectroscopy of an intracerebral glioma in rat brain: assignment of resonances. *J Neurochem*, 1994, 62: 166-179.
23. Candiota A.P., Majós C., Bassols A., Cabanas M.E., Acebes J.J., Quintero M.R., Arús C.: Assignment of the 2.03 ppm resonance in *in vivo* 1H MRS of human brain tumour cystic fluid: contribution of macromolecules *Magn Reson Mater Phys MAGMA*, 2004, 17: 36-46.
24. Candiota A.P.: PhD thesis (2004) (Contribució a la millora del diagnòstic i de la valoració pronòstica de tumors cerebrals humans) http://www.tdx.cesca.es/ TDX-0714105-173443/.
25. Julia-Sape M., Acosta D., Mier M., Arus C., Watson D.; INTERPRET consortium: A multi-centre, web-accessible and quality control-checked database of *in vivo* MR spectra of brain tumour patients. *MAGMA*, 2006, 19: 22-33.
26. Coates H.B., McLauchlan K.A., Campbell I.D., McColl C.E.: Proton spin lattice relaxation time measurements at 90MHz and 270 MHz. *Biochim Biophys Acta*, 1973, 310: 1-10.
27. Frahm J., Bruhn H., Gyngell M.L., Merboldt K.D., Hänicke W., Sauter R.: Localized proton NMR spectroscopy in different regions of the human brain *in vivo*. Relaxation times and concentrations of cerebral metabolites. *Magn Reson Med*, 1989, 11: 47-63.
28. Choi C.G., Frahm J.: Localized proton MRS of the human hippocampus : metabolite concentrations and relaxation times. *Magn Reson Med*, 1999, 41: 204-207.
29. van der Graaf M., Julià -Sapé M., Howe F.A., Ziegler A., Majós C., Moreno-Torres A., Rijpkema M., Acosta D., Opstad K.S., van der Meulen Y.M., Arús C., Heerschap A.: MRS quality assessment in a multicentre study on MRS-based classification of brain tumours. *NMR Biomed*, 2006, 21: 148-158.
30. Kim H., Wild J.M., Allen P.S.: Strategy for the Spectral Filtering of Myo-Inositol and Other Strongly Coupled Spins. *Magn Reson Med*, 2004, 51: 263-272.
31. Prescot A.P., deB Frederick B., Wang L., Brown J., Jensen J.E., Kaufman M.J., and Renshaw P.F: *In vivo* Detection of Brain Glycine with Echo-Time-Averaged 1H Magnetic Resonance Spectroscopy at 4.0 T. *Magn Reson Med*, 2006, 55: 681-686.
32. Choi C., Bhardwaj P.P., Seres P., Kalra S., Tibbo P.G., Coupland N.J.: Measurement of glycine in human brain by triple refocusing 1H-MRS in vivo at 3.0T. *Magn Reson Med*, 2008, 59: 59-64.
33. Gambarota G., Mekle R., Xin L., Hergt M., van der Zwaag W., Krueger G., Gruetter R.: In vivo measurement of glycine with short echotime 1H MRS in human brain at 7 T. *MAGMA*, 2009, 22: 1-4.
34. Bobek-Billewicz B., Hebda A., Stasik-Pres G., Majchrzak K., Zmuda E., Trojanowska A.: Measurement of glycine in a brain and brain tumors by means of 1H MRS. *Folia Neuropathol*, 2010, 48: 190-199.
35. Hattingen E., Lanfermann H., Quick J., Franz K., Zanella F.E., Pilatus U.: 1H MR spectroscopic imaging with short and long echo time to discriminate glycine in glial tumours. *MAGMA*, 2009, 22: 33-41.
36. Kaufman M.J., Prescot A.P., Ongur D., Evins A.E., Barros T.L., Medeiros C.L., Covell J., Wang L., Fava M., Renshaw P.F.: Oral glycine administration increases brain glycine/creatine ratios in men: a proton magnetic resonance spectroscopy study. *Psychiatry Res*, 2009: 173: 143-149.
37. Majós C., Julià-Sapé M., Alonso J., Serrallonga M., Aguilera C., Acebes J.J., Arús C., Gili J.: Tumor classification by proton MR spectroscopy: comparison of diagnostic accuracy at short and long TE. *AJNR Am J Neuroradiol*, 2004, 25: 1696-704.
38. Majós C., Julià-Sapé M. et al.: Proton magnetic resonance spectroscopy provides revelant prognostic information in high-grade astrocytomas. *AJNR*, 2011, 32: 74-80
39 García-Gómez J.M., Tortajada S., Vidal C., Julià-Sapé M., Luts J., Moreno-Torres A., Van Huffel S., Arús C., Robles M.: The effect of combining two echo times in automatic brain tumor classification by MRS. *NMR Biomed*, 2008, 21: 1112-1125.
40. Kleihues P., Ohgaki H.: Primary and secondary glioblastomas: from con-

cept to clinical diagnosis. *Neuro-Oncology*, 1999, 1: 44-51.
41. Mischel P.S., Nelson S.F., Cloughesy T.F.: Molecular analysis of glioblastoma: pathway profiling and its implications for patient therapy. *Cancer Biol Ther*, 2003, 2 : 242-247.
42. Martinez-Bisbal M.C., Marti-Bonmati L., Piquer J., Revert A., Ferrer P., Llacer J.L., Piotto M., Assemat O., Celda B.: 1H and 13C HR-MAS spectroscopy of intact biopsy samples ex vivo and *in vivo* 1H MRS study of human high grade gliomas. *NMR Biomed*, 2004, 17: 191-205.
43. Peeling J., Sutherland G.: High-resolution 1H NMR spectroscopy studies of extracts of human cerebral neoplasms. *Magn Reson Med*, 1992, 24: 123-136
44. Kinoshita Y., Yokota A.: Absolute concentrations of metabolites inhuman brain tumors using in vitro proton magnetic resonance spectroscopy. *NMR Biomed*, 1997, 10: 2-12.
45. Roda J.M., Pascual J.M., Carceller F., González-Llanos F., Pérez-Higueras A., Solivera J., Barrios L., Cerdán S.: Nonhistological diagnosis of human cerebral tumors by 1H magnetic resonance spectroscopy and amino acid analysis. *Clin Cancer Res*, 2000, 6: 3983-3993.
46. Carpinelli G., Carapella C.M., Palombi L., Raus L., Caroli F., Podo F.: Differentiation of glioblastoma multiforme from astrocytomas by in vitro 1H MRS analysis of human brain tumors. *Anticancer Res*, 1996, 16: 1559-1563.
47. Righi V., Mucci A., Schenetti L., Bacci A., Agati R., Leonardi M., Schiavina R., Martorana G., Liguori G., Calabrese C., Boschetti E., Bonora S., Tugnoli V.: Identification of mobile lipids in human cancer tissues by ex vivo diffusion edited HR-MAS MRS. *Oncol Rep*, 2009 22: 1493-1496.
48. Wright A.J., Fellows G.A., Griffiths J.R., Wilson M., Bell B.A., Howe F.A.: Ex-vivo HRMAS of adult brain tumours: metabolite quantification and assignment of tumour biomarkers. *Mol Cancer.*, 2010, 9: 66.
49. Lehnhardt F.G., Bock C., Röhn G., Ernestus R.I., Hoehn M.: Metabolic differences between primary and recurrent human brain tumors: a 1H NMR spectroscopic investigation. *NMR Biomed*, 2005, 18: 371-382.
50. Davies N.P., Wilson M., Natarajan K., Sun Y., MacPherson L., Brundler M.A., Arvanitis TN., Grundy R.G., Peet A.C.: Non-invasive detection of glycine as a biomarker of malignancy in childhood brain tumours using in-vivo 1H MRS at 1.5 tesla confirmed by ex-vivo high-resolution magic-angle spinning NMR. *NMR Biomed*, 2010, 23: 80-87.
51. Zhang K., Weinberg J.M., Venkatachalam M.A., Dong Z.: Glycine protection of PC-12 cells against injury by ATP-depletion. *Neurochem Res*, 2003, 28: 893-901.
52. Nishimura Y., Lemasters J.J.: Glycine blocks opening of a death channel in cultured hepatic sinusoidal endothelial cells during chemical hypoxia. *Cell Death Differ*, 2001, 8: 850-858.
53. Ruiz-Meana M., Pina P., Garcia-Dorado D., Rodriguez-Sinovas A., Barba I., Miro-Casas E., Mirabet M., Soler-Soler J.: Glycine protects cardiomyocytes against lethal reoxygenation injury by inhibiting mitochondrial permeability transition. *J Physiol*, 2004, 558(Pt 3): 873-882.
54. Valverde D., Quintero M.R., Candiota A.P., Badiella L.I., Cabañas M.E., Arús C.: Analysis of the changes in the ^{1}H NMR PCA extract pattern of C6 cells with growth curve stage. *NMR Biomed*, 2006, 19: 223-230.